Int. J. Heat Mass Transfer. Vol. 30, No. 9, pp. 1773–1785, 1987
Printed in Great Britain

0017–9310/87 $3.00 + 0.00
Pergamon Journals Ltd.

Vaporization of a liquid by direct contact in another immiscible liquid
Part I: vaporization of a single droplet
Part II: vaporization of rising multidroplets

L. TADRIST, I. SHEHU DISO, R. SANTINI and J. PANTALONI
Laboratoire des Systèmes énergétiques et Transferts Thermiques, Université de Provence, C.N.R.S. UA 1168, Centre St-Jérôme, rue H. Poincaré, 13397 Marseille Cedex 13, France

(*Received* 17 *March* 1986 *and in final form* 5 *September* 1986)

Abstract—The present work is an experimental and theoretical study of the vaporization by direct contact of refrigerant R113 and n-pentane dispersed into a column of water flowing countercurrently. The vaporization of a single droplet in a stagnant liquid medium, and the evaporation of a multidroplet flowing system are studied. A formalism has been developed to determine the effective exchange surface for the bubble–droplet during its rise in an immiscible liquid. The numerical results are in good agreement with the experiments. The mechanical equilibrium of a bubble–droplet was studied when considering only the surface tension forces. The results obtained in the precedent analysis about the liquid–liquid area estimation were explained. Experiments were performed to investigate the influence of the different parameters on the behaviour of the direct contact vapour generator. A dimensional analysis based on characteristic transfer times was done. From this point of view correlations were established for determining the volumetric heat transfer coefficient and the exchange efficiency. For a multidroplet flowing system an analytical model was proposed giving the evolution of the void fraction and the temperature of each fluid along the exchange column. Experimental and numerical results were compared.

INTRODUCTION

THE RECENT developments on heat transfer by direct contact between two fluids associated with the phase change of one of the fluids have shown many advantages. Due to the higher effective heat transfer coefficient, relative simplicity of design and absence of the scaling surfaces associated with direct contact evaporators and condensers, this type of heat exchanger is particularly suitable for the vaporization of thermal energy at low and moderately high temperatures. Applications include geothermal heat recovery, sea water desalination, waste heat recovery and energy storage systems [1, 2]. They can also be found in many pilot electric plants [3, 4]. The experience acquired with direct contact heat exchangers where one of the liquids changes phase shows that the best performance is obtained when the dispersed liquid is the phase change fluid (solidification or vaporization) [1, 2, 5].

A good understanding of the various mechanisms implemented in such heat exchangers is necessary for sizing direct-contact boilers and condensers and for determining the correlations between the fundamental characteristic parameters. Due to lack of data for sizing these exchangers, Honegger [7] and Wilke *et al.* [8] used correlations relative to liquid–liquid systems. Wilke *et al.* [8] studied experimentally the variations of the volumetric heat transfer coefficient vs dispersed and continuous phase flow rates for the sea water–aroclor system. A similar study was carried out by Sideman and Gat [9] with the pentane–water couple for $(T_c - T_{sat}) < 1.5°C$. Smith *et al.* [10] attempted to calculate the volumetric heat transfer coefficient for direct contact evaporation from an analytical model. This paper constitutes a study of the fundamental mechanisms governing the heat and momentum transfers of a boiling drop in another immiscible liquid, and an experimental study of direct contact evaporation in spray columns. The experiments are conducted with Freon 113–water and n-pentane–water couples in which the first fluid is evaporated in the water. Experimental observations show that the n-pentane and Freon 113 drops obtained by dispersion vaporize with a constant mass, i.e. the vapour bubble remains attached to the liquid sheath.

In the absence of bubble-forming nuclei; drops, suspended or rising in another immiscible liquid, can be highly superheated [11–13]. In this case, evaporation occurs explosively and is characterized by a 'ping' sound. This phenomenon corresponds to the metastable states of the phase change. To avoid this superheating, several authors [14, 15] favoured nucleation by injection of tiny bubbles of air. Much research has been done to study the phenomenon of a single moving drop vaporizing in a stagnant column of immiscible liquid. Experimental investigations of this problem have been reported for a number of couples of liquids and conditions: n-pentane–water, butane–water, pentane–glycerol [12, 14–17]. Expressions of the heat transfer coefficient of a vaporizing drop were determined from theoretical and experimental studies [14, 18–21]. Much work has also been carried out to study the evolution (velocity and

NOMENCLATURE

A	column cross-section
C	specific heat
C_d	drag coefficient
D	drop diameter
d	hole diameter
F	force
g	acceleration due to gravity
H_v	volumetric heat transfer coefficient
h	superficial heat transfer coefficient
H	enthalpy
Ja	Jacob number
k	model coefficient
$k\beta$	effective half opening angle
L_c	continuous phase head
L_d	multiphase mixture head
L_v	latent heat of vaporization
M	molecular weight
m	mass
$\dot{m}$	mass flow rate
N	number density of bubbles, drops or bubble–droplets
$\dot{n}_p$	drop number flow rate
n_h	number of holes
Nu	Nusselt number
P	pressure
Pe	Peclet number
Pr	Prandtl number
Q	heat flow rate
R, r	radius
R_1, R_2, R_3	radii of curvature
Re	Reynolds number, U_pD/ν_c
S_{ex}	exchange area
s	area
T	temperature
ΔT	$T_c - T_{sat}$
ΔT_1	$T_{ce} - T_{ds}$
ΔT_2	$T_{cs} - T_{de}$
ΔT_m	$(\Delta T_1 - \Delta T_2)/\log(\Delta T_1/\Delta T_2)$
t	time
U, u	velocity
v	volume
x	vaporization ratio, m_v/m_T
x_v	vapour ratio, v_v/v_T
X_w	coefficient of drag
z	abscissa.

Greek symbols

α	dispersed phase void fraction
$\bar{\alpha}$	mean void fraction, $(L_d - L_c)/L_d$
β, ω	contact angles
$\beta_1, \beta_2, \beta_3$	angles
ε	exchanger efficiency
η	humidity
λ	thermal conductivity
μ	dynamic viscosity
ν	kinematic viscosity
ρ	mass density
σ	interfacial tension
τ	characteristic time
ψ	volumetric flow rate.

Subscripts

c	continuous phase
d	dispersed phase
e	inlet
i	internal
l	liquid
m	mass
min	minimum
p	drop, bubble or bubble–droplet
r	relative
rt	relaxation time
s	outlet
sat	saturation
T	total
th	thermal
v	vapour
w	water
0	initial
∞	infinity.

growth) of a bubble–droplet [14, 18, 22, 23]. The theoretical results obtained in ref. [22] were, however, not in good agreement with the experimental results [14]. This disagreement is reported [18] to be due to the heat transfer coefficient.

In the first part of this paper we present a study on the vaporization of a moving bubble–droplet and the results of an analysis concerning the mechanical equilibrium between a droplet and its vapour bubble. In the second part, we present a study about the characterization of the main parameters governing the evaporation by direct contact in a spray column.

I. VAPORIZATION OF A SINGLE DROPLET

I.1. *Vaporization of a Bubble–Droplet Moving in Another Immiscible Liquid*

Equations governing the motion of a drop in another fluid

In this section we make the basic assumption that the drop remains spherical. The governing equation is

$$d_t(m_0\mathbf{U}_p) = \mathbf{F}_v + \mathbf{F}_s \quad (1)$$

where d_t is the differential operator (d/dt), and $\mathbf{F}_v$ and

$\mathbf{F}_s$ are the volume and surface forces acting on the bubble–droplet, respectively.

For potential flow ($\mu_c = 0$)

$$\mathbf{F}_s = -(1/2)\mathrm{d}_t(\rho_c \mathbf{u}_r v_p) + \rho_c v_p \mathrm{d}_t \mathbf{u}_c. \quad (2)$$

For Stokes type flow ($Re_p < 1$)

$$\mathbf{F}_s = -6\pi R_p v_c \mathbf{u}_r - (1/2)\mathrm{d}_t(\rho_c \mathbf{u}_r v_p) + \rho_c v_p \mathrm{d}_t \mathbf{u}_c + (3/2)D^2(\rho_c \pi \mu_c)^{1/2} \int \mathrm{d}_t \mathbf{u}_r \, \mathrm{d}s/(t-s)^{1/2}. \quad (3)$$

In practice, few regimes correspond to either of the limit cases ($\mu_c = 0$ or $Re_p < 1$). For $Re_p > 200$, some authors [24] assume that the flow around a drop may be reasonably considered potential. Depending on the Reynolds number Re_p, and according to ref. [25], it is preferable to adapt either of the above expressions for $\mathbf{F}_s$ by introducing appropriate correction factors.

In the light of these remarks, and considering the size and velocity of the drops in the column, the equation of motion of a bubble–droplet in a stagnant liquid medium is

$$(m_0 + 2\pi\rho_c R_p^3/3)\mathrm{d}_t(\mathbf{U}_p) = (-m_0 g + 4\pi R_p^3 \rho_c g/3) - 2\pi\rho_c \mathbf{U}_p R_p^2 \mathrm{d}_t R_p - \pi\rho_c R_p^2 \mathbf{U}_p^2 C_d/2. \quad (4)$$

Since the bubble has a continuously varying volume due to the evaporation of the liquid sheath, its growth can be described by the Rayleigh–Plesset equation

$$R_p^2 \mathrm{d}_t^2 R_p + (3/2)R_p(\mathrm{d}_t R_p)^2 = [P(R_p) - P_\infty]R_p/\rho_c - 4\nu_c \mathrm{d}_t R_p + \mathbf{u}_r^2 R_p/4 \quad (5)$$

where the pressure on the liquid side $P(R_p)$ is

$$P(R_p) = P_i - 2\sigma/R_p \quad \text{and} \quad P_i = P_i(T).$$

Energy conservation equation

When mass conservation is supposed (the bubble does not detach from the droplet) and heat transfer equals the heat of vaporization, the energy equation is

$$\mathrm{d}_t v_p = QL_v^{-1}(\rho_{dv}^{-1} - \rho_{dl}^{-1}) \quad (6)$$

or

$$4\pi R_p^2 \mathrm{d}_t R_p = QL_v^{-1}(\rho_{dv}^{-1} - \rho_{dl}^{-1}) \quad (6')$$

with

$$Q = S_{ex} h(T_c - T_{sat}).$$

The initial conditions are at $t = 0$:

$$U_p(0) = U_0 \quad \text{and} \quad R_p(0) = R_0 \quad (7)$$

and the final condition at t_T:

$$R_p(t_T) = R_p(0)[\rho_{dl}/\rho_{dv}]^{1/3}$$

where t_T is the total vaporization time.

Results

The set of equations (4)–(7), together with the equation of state were solved numerically and found to give the rise velocity and the vaporization ratio as functions of time. In order to solve these equations, the heat transfer and drag coefficients must, however, be known.

Drag coefficient. In spite of the lack of data on drag coefficients for a bubble–droplet moving in another immiscible liquid, the correlation obtained by Haberman and Morton [26] for air bubbles moving in water may reasonably be used in the case of a bubble–droplet when the vaporization ratio x is greater than 1%, since in this case the corresponding volumetric vapour ratio is about unity ($x_v \simeq 1$).

Results with classical heat transfer coefficients

The theoretical heat transfer coefficients given by Sideman and Taitel [14]: $Nu = 0.272Pe^{1/2}$; and later modified by Battya *et al.* [18]: $Nu = 0.64Ja^{-0.35}Pe^{1/2}$ were used in our analysis. These heat transfer coefficients are mean overall coefficients, i.e. averaged over the whole bubble–droplet area. Comparison with our theoretical and experimental results [14] revealed some significant discrepancies. Figure 1 shows an example of these results.

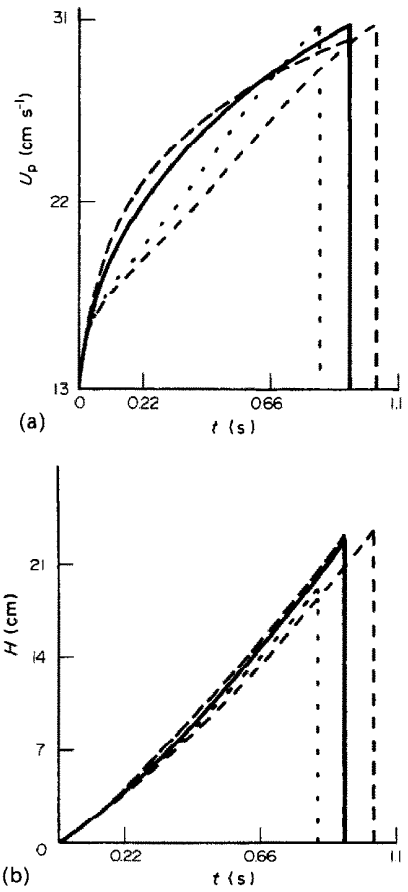

FIG. 1. Velocity U_p (a) and height H (b) of a bubble–droplet vs time t for the different analysis ($\Delta T = 5.7°C$; $D_0 = 0.349$ cm): ———, experimental results of Sideman and Taitel [14]; ———, present analysis; - - - - - -, theoretical result with heat transfer coefficient given in ref. [14]; — — — —, theoretical result with heat transfer coefficient given by Battya *et al.* [18].

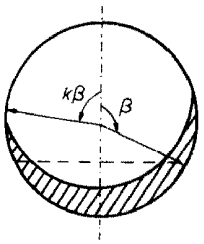

FIG. 2. Supposed bubble–droplet geometry for the model. This figure shows the definition of the coefficient k which gives the effective heat exchange area: ——, plane interface between the liquid and its vapour; ———, interface given with the correction factor k.

Present mode

In agreement with many authors [14, 21, 27], we assume that heat transfer takes place only at the liquid–liquid interface with the corresponding heat transfer coefficient. The determination of the effective heat exchange area depends on the choice of the bubble–droplet geometry. The simplest assumption is to consider that the inner liquid–vapour interface is plane (Fig. 2). The total evaporation times obtained from this model are, however, overestimated compared with the corresponding experimental values of ref. [14]. In the absence of any satisfying model, we determine the effective liquid–liquid area by taking into account the experimental results of the latter authors where we supposed that the bubble–droplet geometry is as illustrated in Fig. 2. This effective heat transfer area is determined such that the *total vaporization time equals the experimental value* reported in ref. [14]. The effective area is therefore given as

$$s_1 = 2\pi R^2(1+\cos k\beta) \tag{8}$$

where the coefficient k is the unknown parameter introduced to account for the effective surface compared to its plane interface value ($k = 1$). After numerous experiments (approx. 40) with the n-pentane–water system under the following conditions:

initial drop diameter: $2\text{ mm} < D_0 < 4\text{ mm}$

superheat $\Delta T = (T_c - T_{sat})$: $1.5^\circ\text{C} < \Delta T < 15^\circ\text{C}$

the values obtained for the parameter k are such that $0.75 < k < 0.85$. The rise velocity and height profiles as functions of time given by this model are in better agreement with experiments described in ref. [14], as shown in Fig. 1. This agreement shows that the assumption of a liquid–liquid heat transfer through a surface different from its corresponding plane interface value, gives a coherent model that can correctly describe the bubble–droplet vaporization. Moreover, the value of the coefficient k remains approximately constant for all the different experiments. It is probable that this result characterizes 'an' equilibrium state of a moving bubble–droplet vaporizing in another immiscible liquid. Raina and Grover [27] developed a model for determining the liquid–liquid area by introducing the effect of viscous shear on the spreading of dispersed liquid over the bubble surface.

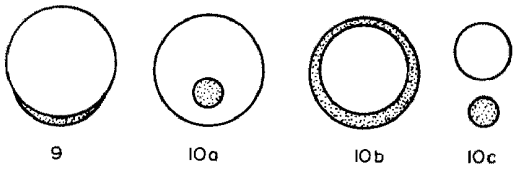

FIG. 3. Configurations of the drop (⊗) with its bubble (○) corresponding to relations (9), (10a), (10b), and (10c).

However, their relation on the equilibrium location of the end of the thin film can only be satisfied for high velocities of the bubble–droplet (n-pentane–water $U > 14\text{ m s}^{-1}$) or for very small spreading coefficients $S_d = \sigma_{cv} - (\sigma_{dc} + \sigma_{dv})$.

Our analysis of a moving bubble–droplet vaporizing in another immiscible liquid gives satisfying results. This analysis necessitates the determination of the coefficient k from the experiments. For this reason an attempt is made to develop a more general model which gives the liquid–liquid area of a bubble droplet from its mechanical equilibrium.

I.2. *Mechanical Equilibrium of a Bubble–Droplet*

In this section, we present an analysis, based on the sole consideration of the interfacial and superficial tensions, for the determination of the different configurations of a bubble–droplet as well as of the liquid–liquid exchange area when the bubble remains attached to its droplet.

For theoretical analysis, we make the following assumptions:

(a) absence of any fluid motion (or negligible dynamic effects);

(b) neglect buoyancy effects.

Under these conditions the jump of stress is equal to the pressure difference across each interface. Assuming that the interfacial tensions are constant, each interface is therefore spherical. The mechanical equilibrium is then defined by the following relationship:

$$2\pi r(\boldsymbol{\sigma}_{cv} + \boldsymbol{\sigma}_{cd} + \boldsymbol{\sigma}_{dv}) = \mathbf{0}. \tag{9}$$

When this condition is not satisfied, a common point between the three media cannot exist. Three cases are then possible:

(1) $$\sigma_{cd} > \sigma_{cv} + \sigma_{dv} \tag{10a}$$

The vapour bubble surrounds the droplet.

(2) $$\sigma_{dv} > \sigma_{cd} + \sigma_{cv} \tag{10b}$$

The vapour bubble detaches from the droplet.

(3) $$\sigma_{cv} > \sigma_{cd} + \sigma_{dv} \tag{10c}$$

The vapour bubble enters into the drop.

Figure 3 shows the different configurations corresponding to the above relations.

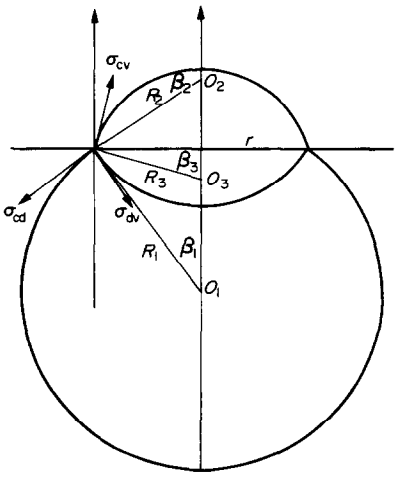

FIG. 4. Analytical model: bubble–droplet geometry with definitions of the various parameters.

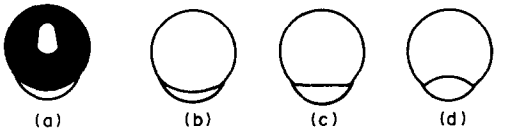

FIG. 5. Bubble–droplet photography (a) given in ref. [21] compared to the geometry of the bubble–droplet obtained with the model for different values of σ_{dc}, (b) $\sigma_{dc} = 37$ dyn cm^{-1}, (c) $\sigma_{dc} = 40$ dyn cm^{-1}, (d) $\sigma_{dc} = 62$ dyn cm^{-1}. These results concern the furan–glycerol couple and correspond to a vaporization ratio of 3.2%.

For the case where the bubble remains attached to the droplet it is possible to determine vaporization ratios x, the bubble–droplet geometry as characterized by its radii of curvature and to deduce the liquid–liquid area vs x. Figure 4 shows the bubble–droplet geometry and gives the different parameters used. In this case the set of equations governing the mechanical equilibrium of the bubble–droplet is defined by the following relationships:

$$-\sigma_{cv}\sin\beta_3+\sigma_{dc}\sin\beta_1+\sigma_{dv}\sin\beta_2=0 \quad (11)$$

$$\sigma_{cv}\cos\beta_3-\sigma_{dc}\cos\beta_1-\sigma_{dv}\cos\beta_2=0 \quad (12)$$

$$R_1\sin\beta_1=R_2\sin\beta_2=R_3\sin\beta_3=r \quad (13)$$

$$v_l=(2/3)\pi[R_1^3(1+(3/2)\cos\beta_1-(1/2)\cos^3\beta_1)-R_2^3(1+(3/2)\cos\beta_2-(1/2)\cos^3\beta_2)] \quad (14)$$

$$v_v=(2/3)\pi[R_3^3(1-(3/2)\cos\beta_3+(1/2)\cos^3\beta_3)+R_2^3(1+(3/2)\cos\beta_2-(1/2)\cos^3\beta_2)]. \quad (15)$$

The contact angles $\omega=\beta_2-\beta_1$ and $\beta=\beta_3-\beta_1$ are related to the interfacial tensions by the following relations:

$$\cos(\omega)=(\sigma_{cv}^2-\sigma_{dc}^2-\sigma_{dv}^2)/(2\sigma_{dc}\sigma_{dv}) \quad (16)$$

$$\cos(\beta)=(\sigma_{cv}^2+\sigma_{dc}^2-\sigma_{dv}^2)/(2\sigma_{cv}\sigma_{dc}). \quad (17)$$

The angle β_1 is determined from

$$v_l/v_v=(A-B)/(B+C) \quad (18)$$

where

$$A=[1+(3/2)\cos\beta_1-(1/2)\cos^3\beta_1]$$

$$B=[\sin^3\beta_1/\sin^3(\beta_1+\omega)][1+(3/2)\cos(\beta_1+\omega)-(1/2)\cos^3(\beta_1+\omega)]$$

$$C=[\sin^3\beta_1/\sin^3(\beta_1+\beta)][1-(3/2)\cos(\beta_1+\beta)+(1/2)\cos^3(\beta_1+\beta)].$$

For given values of the interfacial tensions (σ_{ij}) and vapour ratio, the resolution of the above set of equations gives the contact angles and the three radii (R_i).

For the furan–aqueous glycerol couple studied by Tochitani *et al.* [15], values of the surface tension are: $\sigma_{cv} = 62$ dyn cm^{-1}, $\sigma_{dv} = 26$ dyn cm^{-1}, and the interfacial tension $\sigma_{dc} = 31$ dyn cm^{-1}. For these values satisfying inequality (10c) the vapour bubble will be engulfed by the drop. This fact was, however, not observed experimentally. We have therefore adjusted one of the three values, σ_{dc} for example, so as to satisfy equation (9). Figure 5 shows the shape of the bubble–droplet for three such values of σ_{dc}. The internal interface depends strongly on the σ_{dc} value. If $\sigma_{dc} > (\sigma_{cv}-\sigma_{dv})$ the calculated curvature of the inner interface is similar to the experimental curvature (Fig. 5). For this case we have numerically simulated the evolution of the vaporizing bubble–droplet. Figure 6 compares the results of our model with the experiments of ref. [15].

A comparison of the evolution of the specific liquid–liquid area obtained for different situations is shown in Fig. 7: from our analysis, the plane bubble–drop interface and experimental points obtained by Tochitani *et al.* [15]. The specific areas obtained experimentally are greater than those corresponding to a plane bubble–droplet interface at the onset of vaporization. The opposite is true at greater vaporization ratios. This behaviour is taken into account by our mechanical equilibrium analysis.

For the n-pentane–water system, the interfacial tensions are: $\sigma_{cv} = 76$ dyn cm^{-1} at 36°C, $\sigma_{dv} = 18.5$ dyn cm^{-1} at 20°C, $\sigma_{cd} = 37$ dyn cm^{-1} at 30°C. These values correspond nevertheless to inequality (10c). The bubble should enter into the drop. This means that interfacial tensions alone cannot describe the bubble–droplet equilibrium. We therefore conclude that other external forces, in particular the gravitational forces, must be taken into account.

In the following section we present an experimental study the object of which is to identify the influence of the characteristic parameters on the heat exchange and to simulate numerically the function of this type of evaporator.

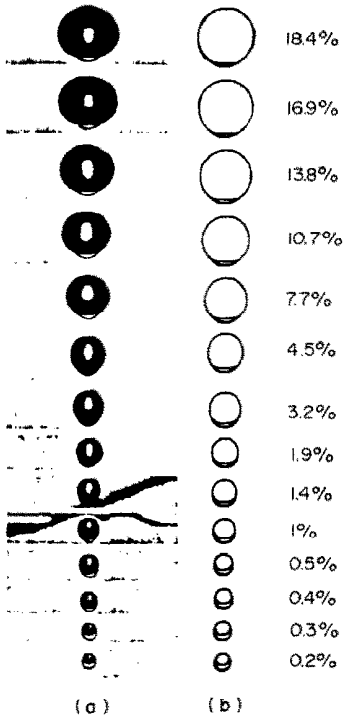

FIG. 6. Qualitative comparison between the photographs of a vaporizing furan drop in glycerol and the geometry of the bubble droplet predicted by our model for different vaporization ratios x. The values of the surface tension are, $\sigma_{cv} = 62$ dyn cm^{-1}, $\sigma_{dv} = 26$ dyn cm^{-1} and the interfacial tension $\sigma_{dc} = 31$ dyn cm^{-1}: (a) the photographs were obtained by Tochitani *et al.* [21]; (b) numerical solutions obtained from our model.

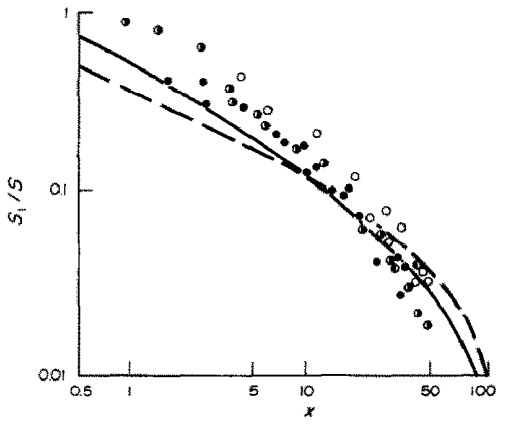

FIG. 7. Specific liquid area S_i/S of the bubble–droplet vs the vaporization ratio x: ———, present analysis; — — —, plane interface; ○, experimental results ref. [21].

II. VAPORIZATION OF RISING MULTIDROPLETS

II.1. *Description Operation of the Experiment*

Description

Figure 8 shows the schematic diagram of the experimental apparatus consisting of four main components.

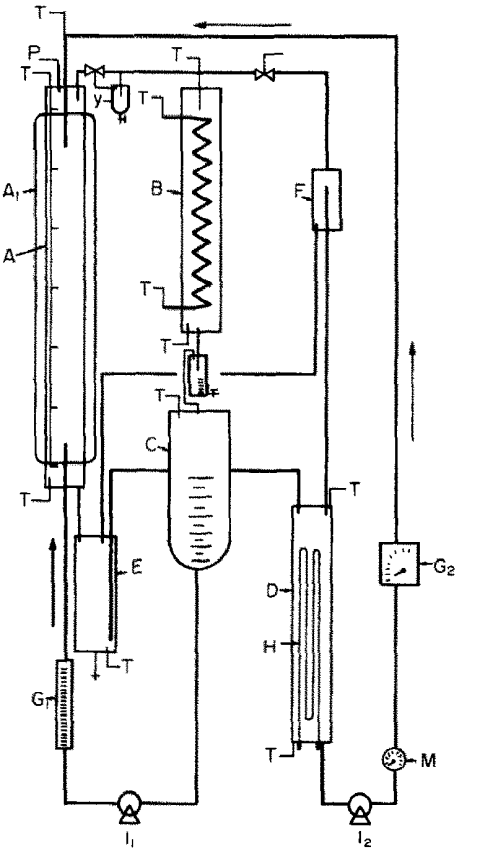

FIG. 8. Schematic diagram of the apparatus: A, exchange column; A_1, thermal insulation; B, condenser; C, dispersed phase receiver; D, water heater; E–F, separators; G_1–G_2, flowmeters; l_1–l_2, pumps; T, thermocouples; P–M, pressure gauges; Y, cyclone.

(1) A storage vessel C containing the volatile liquid.

(2) The exchange column consisting of a glass cylinder A 100 mm in diameter and 1000 mm high. Vacuum drawn in the jacket A_1 surrounding the exchange column assured the insulation of the latter element.

(3) The water heater D was a glass cylinder 100 mm in diameter and 600 mm high housing an electric resistance the power of which is about 7 kW.

(4) A classical condenser B (type shell and tube) cooled by cold tap water.

Elements E and F allowed the separation of the dispersed phase from the continuous phase when entrainment occurs. A cyclone Y was inserted between the exchange column and the condenser. These elements were connected by 16 mm glass tubing.

The injection of the dispersed phase was realized with thirty-seven 1 mm diameter holes while that of the continuous phase with a distribution plate containing 100 holes of 1.5 mm diameter.

The power of this loop is about 7 kW and functions continuously at atmospheric pressure and for a temperature range of 30–90°C. The flow rates of the fluids were monitored. Temperatures were taken at several points in the system with nickel chrome–nickel thermocouples.

Operation

The continuous phase enters at the top of the spray column through the distribution plate. It is collected at the lower part, passes through the separator and returns to the water heater. The dispersed phase is percolated through 1 mm diameter holes in an insulated distribution plate at the bottom of the column. At the contact of the hotter continuous phase, the dispersed phase is first heated, then begins to vaporize. By the time it reaches the top of the active volume, it has completely vaporized. The generated vapour leaves the spray column and passes through a cyclone then goes to the condenser where it is liquified. This liquid is collected in the storage vessel after passing through a graduated test-tube used to monitor the entrained continuous phase.

II.2. *Experimental Results*

Dragging of phases

The experiments have revealed the influence of the mode of injection of the dispersed phase on the heat transfer in the system. Small diameter drops were found to allow better heat transfer between the two phases. Castex [28] showed that these drop sizes are easily obtained from turbulent jets. Nevertheless, for this jet regime, a wide range of drop sizes was observed. The smallest drops of diameter below a critical value, are carried along with the continuous phase. Because the distribution of drop sizes is narrower for laminar jets and drop by drop flow regimes, this effect can be reduced by an appropriate size of the injection holes.

Again we have observed that a fraction of the continuous phase can be found in the vapour circuit. To determine the state in which the continuous phase was carried, a cyclone was inserted in the vapour circuit in order to trap the water droplets. Since very little water was collected, we concluded that it was essentially carried out in vapour form.

For the evaluation of this fraction we make the following simplifying assumptions:

(a) relative humidity is equal to unity;

(b) the vapours are supposed to obey the perfect gas laws.

From these assumptions the evaluation gives a maximal value of the water vapour carried out in the vapour circuit.

The mass fraction of the water contained in the dispersed phase can be expressed as

$$X_w = (M_w/M_d)[P_{sat}/(P_T - P_{sat})]. \quad (19)$$

In the steady state the water vapour flow rate is therefore: $\dot{m}_w = X_w \dot{m}_d$. Figure 9 shows the water vapour mass percentage entrained vs the dispersed phase flow rate. It can be seen that the experimental values are less than the calculated values.

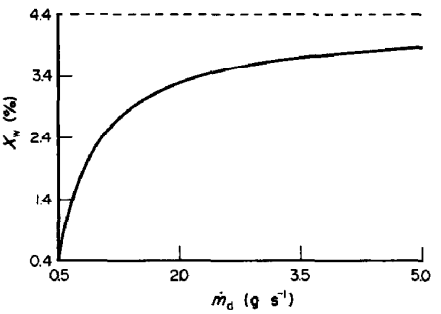

FIG. 9. Entrained continuous phase vapour mass percentage X_w vs dispersed phase mass flow rate $\dot{m}$ for the n-pentane–water couple: ———, experimental results; — — —, evaluation from the vapour pressure assumption.

In general the relative humidity will be equal to unity for times orders of magnitude greater than the n-pentane vapour residence time in the exchange column. However, with increasing dispersed phase flow rates the agitation of the continuous phase is more important, resulting in higher kinetics of evaporation, the mass fraction then tends asymptotically towards its maximum value. This fact explains the curve of Fig. 9.

II.3. *Thermal Analysis*

A global study of the hydrodynamics and thermal conditions in the exchange column was done at different continuous phase heights and flow rates. In general the thermal characteristics of this type of heat exchanger proved to be very interesting. The enthalpy efficiency defined as the ratio of the heat flow rate recovered by the dispersed phase to the heat flow rate given by the continuous phase ($K = Q_d/Q_c$) is always around unity in all our runs. So the heat loss may be considered negligible.

Evaporator efficiency

The exchanger efficiency is defined as the ratio of the transferred heat flow rate to the maximum heat flow rate transferable. When the heat loss in the exchanger is negligible, the efficiency is

$$\begin{aligned}\varepsilon &= Q_c/[(\dot{m}C)_{min}(T_{ce} - T_{de})] \\ &= Q_d/[(\dot{m}C)_{min}(T_{ce} - T_{de})].\end{aligned} \quad (20)$$

The determination of ε requires the knowledge of $(\dot{m}C)_{min}$. When a phase change occurs (in this case evaporation of the dispersed phase) we introduce the notion of an equivalent specific heat C^* defined as

$$\Delta H_d = C_d^*(T_{ds} - T_{de}) = C_{dl}(T_{dv} - T_{de}) + L_v + C_{dv}(T_{ds} - T_{dv}). \quad (21)$$

In our experiments, the values of $(\dot{m}C)_c$ are always greater than $(\dot{m}C^*)_d$ for the two couples in the experiment. Then $(\dot{m}C)_{min} = (\dot{m}C^*)_d$. So the expression of the evaporator efficiency is

$$\varepsilon = (T_{ds} - T_{de})/(T_{ce} - T_{de}). \quad (20')$$

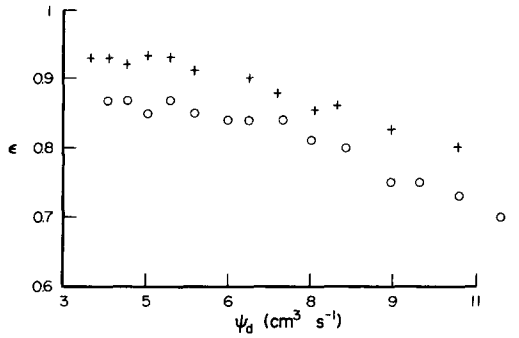

FIG. 10(a). Exchanger efficiency ε vs the dispersed flow rate ψ_d for the Freon 113–water system, for different initial continuous phase heads and for $\psi_c = 27$ cm^3 s^{-1}: +, L_c = 0.20 m; ○, L_c = 0.40 m.

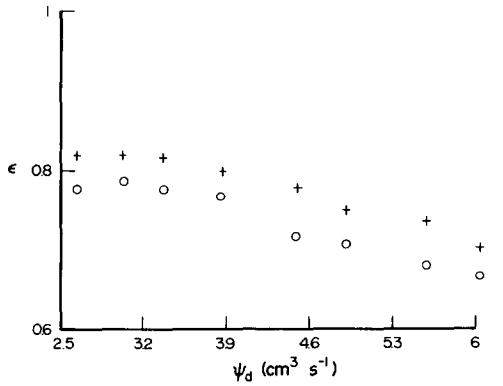

FIG. 10(b). Variation of the exchanger efficiency vs the dispersed flow rate ψ_d (continuous phase flow rate $\psi_c = 76$ cm^3 s^{-1}) for the n-pentane–water system: ○, L_c = 0.20 m; +, L_c = 0.60 m.

Figures 10(a) and (b) show the influence of the dispersed phase flow rate ψ_d and continuous phase heights L_c for the Freon 113–water and n-pentane–water systems.

It can be noted that for the n-pentane–water system the efficiency increases with the continuous phase height while the inverse is true for the Freon 113–water system.

The heat transfers are strongly correlated with the hydrodynamic characteristics. Observation of the behaviour of the flow regime revealed recirculation zones all along the exchange column for the Freon 113–water system. The vortex sizes increase with increasing continuous phase height. The effects of increasing vortex size is to homogenize the temperatures in the whole column. Thus, countercurrent flow is not really established resulting in diminished exchanger efficiency. Conversely, a smaller vortex gives a better exchanger efficiency. These recirculation zones are however not observed with the n-pentane–water system.

The variation of the exchanger efficiency vs the continuous phase flow rate is as shown in Fig. 11 and is similar for the two systems. This figure shows that increasing the continuous phase flow rate does not greatly affect the flow in the exchange column.

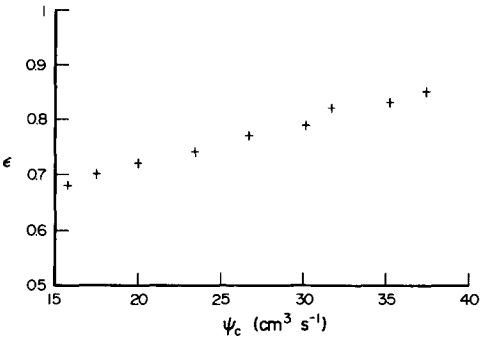

FIG. 11. Variation of the exchanger efficiency vs the continuous phase flow rate ψ_c for the Freon 113–water system and for: $\psi_d = 3$ cm^3 s^{-1}; L_c = 0.40 m.

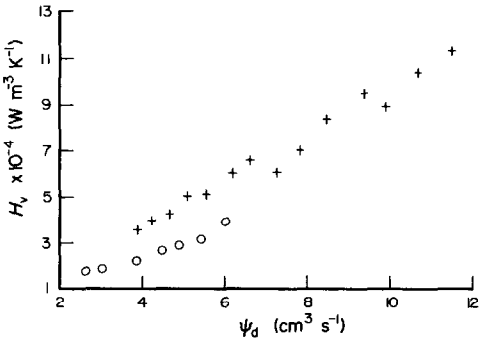

FIG. 12(a). Volumetric heat transfer coefficient H_v vs the dispersed phase flow rate ψ_d ($\psi_c = 76$ cm^3 s^{-1}, L_c = 0.20 m) for the two couples: ○, Freon 113–water; +, n-pentane–water.

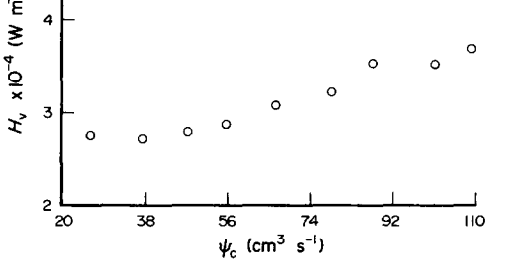

FIG. 12(b). Volumetric heat transfer coefficient H_v vs the continuous phase flow rate ψ_c for the n-pentane–water system: $\psi_d = 6$ cm^3 s^{-1}; L_c = 0.40 m.

Volumetric heat transfer coefficient

The volumetric heat transfer coefficient is defined for this evaporator as

$$H_v = (1-\bar{\alpha})Q_c/(AL_c\Delta T_m). \quad (22)$$

A parametric study of H_v shows a stronger variation with the dispersed phase flow rate as compared to the continuous phase flow rate. Figures 12(a) and (b) show these variations for the two systems studied. It can be noted that values obtained with the n-pentane–water system are higher than those of the Freon 113–water couple. The influence of the continuous phase height on the volumetric coefficient is illustrated in Fig. 13.

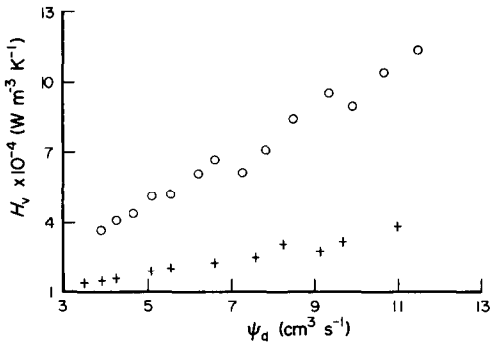

FIG. 13. Variation of the volumetric heat transfer coefficient H_v vs the dispersed phase flow rate ψ_d ($\psi_c = 76$ cm^3 s^{-1}) for the n-pentane–water system: ○, $L_c = 0.20$ m; +, $L_c = 0.60$ m.

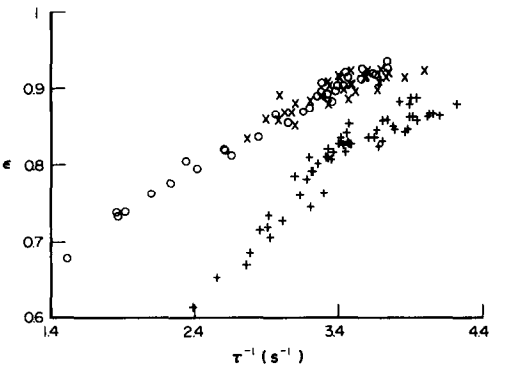

FIG. 14. Variation of the exchanger efficiency ε vs the characteristic parameter τ^{-1} for different continuous phase heads (n-pentane–water system): +, $L_c = 0.20$ m; ○, $L_c = 0.40$ m; ×, $L_c = 0.60$ m.

The above results reveal a high influence of the dispersed phase flow rate on the thermal characteristics of this type of evaporator; and that the better performance of the n-pentane–water system can be attributed to the column hydrodynamics which is conditioned by the density difference of the two phases. Actually, when this difference $(\rho_d - \rho_c)$ does not change sign in the column, the flow remains countercurrent. Inversely if this difference changes sign, the recirculation phenomenon occurs and the flow cannot be considered countercurrent. The maximum value of the volumetric heat transfer coefficient obtained with the Freon 113–water system is about 45 kW m^{-3} °C^{-1} in our experiments. This limit value is conditioned by the dragging of the dispersed phase which is non-negligible at high flow rates. For the n-pentane–water system, however, the maximum value of $H_v = 120$ kW m^{-3} °C^{-1} is limited by the maximum flow rates of the pumps used.

Simplified model

Since it is difficult to determine the individual influences of the given set of parameters governing the functioning of the exchange column, sizing this type of evaporators necessitates a dimensional approach. The dimensional analysis presented here is based on characteristic transfer times.

Optimum heat transfer depends on the significance of the thermal transfer time compared to the residence time in the exchange column. This optimum heat transfer varies directly with residence time and inversely with the thermal transfer time.

From the energy equation $\mathrm{d}_t H = hS_{ex}[T_c(t) - T_p(t)]$ between a droplet or a bubble and the surrounding fluid, together with an enthalpy balance, we obtain by integration the thermal transfer time in each zone:

liquid–liquid zone (1):

$$\tau_{th1} = \tau_{rt1} \log \{(T_{cs} - T_{ed})/[(T_{cs} - T_{sat}) + C_1(T_{sat} - T_{ed})]\}/(1 - C_1)$$

where τ_{rt1} is the thermal relaxation time

$$\tau_{rt1} = m_0 C_{dl}/h_1 s_p \text{ and } C_1 = (\rho_{dl} C_{dl}/\rho_c C_c)(\psi_d/\psi_c);$$

vaporization zone (2)

$$\tau_{th2} = \tau_{rt2} R_0^2/(3a^{2/3})[(1/2)\log[(a^{1/3} + R_v)^3/(a + R_v^3)] + \sqrt{3}Atn[\sqrt{3}R_v/(2a^{1/3} - R_v)]$$

where

$$\tau_{rt2} = \rho_{dv} L_v/h_2 R_0^2 b,$$

$$b = 4\pi\rho_{dv}(\rho_{dl} L_v/\rho_c C_c)(\psi_d/\psi_c)/(3m_0),$$

$$a = (T_{cl} - T_{sat})/b;$$

liquid–vapour zone (3)

$$\tau_{th3} = \tau_{rt3} \log \{(T_{ce} - T_{sat})/[(T_{ce} - T_{ds}) + C_3(T_{ds} - T_{sat})]\}/(1 - C_3)$$

with

$$\tau_{rt3} = m_0 C_{dv}/h_3 s_p \text{ and } C_3 = (\rho_{dl} C_{dv}/\rho_c C_c)(\psi_d/\psi_c).$$

For a drop which vaporizes completely its global characteristic heat transfer time is defined as: $\tau = \Sigma_i \tau_{thi}$.

However, it is not easy to evaluate the droplet–bubble residence time in the column since this depends on the column hydrodynamics and thermal conditions. Nevertheless, it is plain that for a given value of τ (Fig. 14), the exchanger efficiency is a function of continuous phase height and therefore of the transit time.

The volumetric heat transfer coefficient depends however on the characteristic heat transfer time (τ^{-1}) and the drop number flow rate ($\dot{n}_p$). Figure 15 shows the evolution of H_v vs the characteristic parameter ($\dot{n}_p \tau^{-1}$) for different continuous phase heights. The slight scatter in the correlations are probably due to fluctuations of the operating column height.

II.4. *Theoretical Analysis of a Two-phase Flow*

The application presented here involves the flow of three fluid phases. It is desirable to seek a dynamic

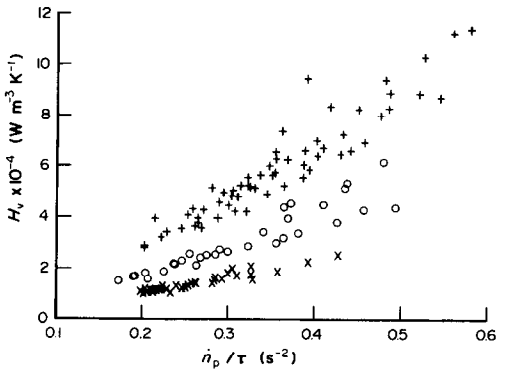

FIG. 15. Volumetric heat transfer coefficient H_v vs the characteristic parameter ($\dot{n}_p\tau^{-1}$) for different continuous phase heads L_c (n-pentane–water system): +, $L_c = 0.20$ m; ○, $L_c = 0.40$ m; ×, $L_c = 0.60$ m.

description of the total flow in order to predict the evolution of the temperature profiles of the two fluids and the void fraction along the column. Considering the complexity of the flow, we make the following simplifying assumptions:

(a) the flow is steady and one-dimensional;
(b) quantities are constant in a cross-section;
(c) bubble–droplets remain spherical and are of the same diameter;
(d) fragmentation and coalescence do not occur;
(e) drops are assumed to behave independently of one another, thus an equation of motion similar to equation (4) may be used.

The analysis can be decomposed into three zones (Z_i), namely: liquid–liquid zone (Z_1), vaporization zone (Z_2), liquid–vapour zone (Z_3).

Liquid–liquid zone

Mass conservation. For the dispersed phase, the mass entering a cross-section of the column per unit time at abscissa z is

$$m(z) = \alpha(z)\rho(z)U_p(z)A.$$

The mass leaving per unit time at abscissa $(z+dz)$ is

$$m(z+dz) = \alpha(z+dz)\rho(z+dz)U_p(z+dz)A.$$

For a constant column cross-section, the mass balance yields from the above relations

$$d_z[\alpha(z)\rho(z)U_p(z)] = 0.$$

Introducing the relation $\alpha(z) = N(z)v_p(z)$ in the precedent and remembering that in this zone $\rho(z)$ and $v_p(z)$ are constant, the mass conservation is as follows:

$$d_z[NU_p] = 0. \quad (23)$$

A similar approach for the continuous phase yields

$$d_z[\alpha_c(z)\rho_c(z)u_c(z)] = 0$$

which can be expressed as

$$(1-Nv_p)d_z(u_c) - u_c v_p d_z(N) = 0. \quad (24)$$

Momentum balance. This equation is similar to equation (4). Since the continuous phase is flowing this equation was modified as follows:

$$U_p(m_0+\rho_c v_p/2)d_z(U_p)+(3/2)U_p\rho_c v_p d_z(u_c) = -\pi C_d\rho_c R_p^2 u_r^2/2+(\rho_c-\rho_p)gv_p. \quad (4')$$

Energy balance. The equations governing the heat transfer for the two phases are

$$d_z(T_p) = Q/(\rho_d C_d U_p v_p) \quad (25)$$

$$d_z(T_c) = -NQ/[(1-Nv_p)u_c\rho_c C_c]. \quad (26)$$

Vaporization zone

In this zone and because of the vaporization, the bubble–droplet grows and its radius is not constant. So the above set of equations is as follows:

$$d_z[NU_p] = 0 \quad (23)$$

$$(1-Nv_p)d_z(u_c) - s_p u_c N d_z(R_p) - u_c v_p d_z(N) = 0 \quad (27)$$

$$U_p(m_0+\rho_c v_p/2)d_z(U_p)+(3/2)U_p\rho_c v_p d_z(u_c) = -\pi C_d\rho_c R_p^2 u_r^2/2+(\rho_c-\rho_p)gv_p^{-1/2}\rho_c u_r U_p s_p d_z(R_p) \quad (28)$$

$$d_z(R_p) = Q(\rho_{dl}-\rho_{dv})/[\rho_{dl}\rho_{dv}L_v s_p U_p] \quad (29)$$

$$d_z(T_c) = -NQ/[(1-Nv_p)u_c\rho_c C_c] \quad (26)$$

$$T_d = T_{sat}.$$

Liquid–vapour zone

The conservation equations for this zone are similar to those defined for the liquid–liquid zone with the corresponding thermophysical properties.

The boundary conditions. These are as follows:

$$T_d(0) = T_{de}; \quad U_p(0) = 4\psi_d/[\pi d_h^2 n_h]; \quad R_p(0) = R_0;$$

$$N(0) = \psi_d/[v(0)U_p(0)A]; \quad u_c(0) = \psi_c/[\alpha_c(0)A].$$

The above set of equations was solved numerically with the appropriate heat transfer and drag coefficients.

(1) *Heat transfer coefficients.* For the first and second zones, the heat transfer coefficient determined in ref. [29] is

$$Nu = hD/\lambda_c = 1.26\{1-\alpha^{5/3}/[2+3\alpha^{5/3}+\alpha^{1/3}(3+2\alpha^{5/3})]\}Re^{1/3}Pr^{1/3}.$$

For the third zone, the heat transfer coefficient between a bubble moving in a liquid given in ref. [20] is

$$Nu = hD/\lambda_c = 0.37Re^{0.6}Pr^{1/2}.$$

(2) *Drag coefficients.* For the liquid–liquid zone the correlation is [30]

$$C_d = 24/Re[1+0.179Re^{0.63}+2.6\times10^{-4}Re^{1.38}].$$

For the vaporization and liquid–vapour zone the Haberman and Morton [26] correlation was used. The profiles of the dispersed phase temperature, continuous phase temperature and void fraction, radius

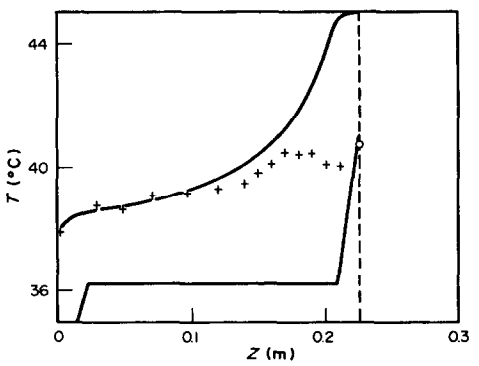

FIG. 16. Temperature profiles along the evaporator in countercurrent flow (n-pentane–water system). The abscissa zero is chosen at the dispersed phase plate ($\psi_d = 4.2$ cm^3 s^{-1}, $\psi_c = 42$ cm^3 s^{-1}, $L_c = 0.20$ m, $D_0 = 0.3$ cm): ———, continuous phase temperature profile $T_c(z)$ obtained numerically; ———, dispersed phase temperature profile $T_d(z)$ obtained numerically; — — —, shows the multiphase mixture head L_d of the active exchange volume obtained numerically and experimentally; +, experimental points of the mixture temperature along the evaporator; ○, measured dispersed phase outlet temperature.

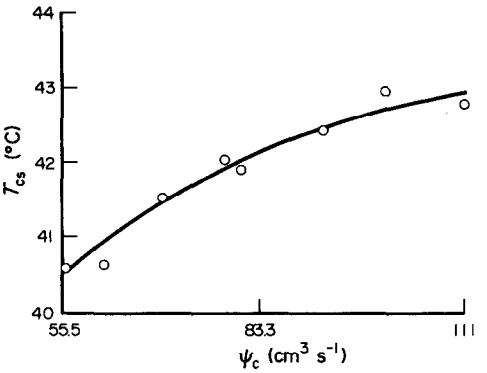

FIG. 17. Comparison between the theoretical and experimental variations of the continuous phase outlet temperatures vs the continuous phase flow rates ψ_c for the n-pentane–water system ($\psi_d = 4.2$ cm^3 s^{-1}, $D_0 = 0.3$ cm, $L_c = 0.20$ cm): ———, simulation results; ○, experimental results.

of the bubble–droplet, and velocity of each phase in the evaporator column were obtained by solving the set of equations using the method of finite differences.

Comparison of computational and experimental results

In Fig. 16 the continuous and dispersed phase temperatures obtained numerically were plotted vs the abscissae z. The temperatures measured with 1 mm diameter nickel chrome–nickel thermocouples all along the column were also plotted.

Close agreement between the estimated and the measured continuous phase temperatures can be noted up to the exchanger column mid-height. Surely, this agreement can be explained by the fact that in this zone, the void fraction is low so the measured temperatures correspond to the actual continuous phase temperatures. Beyond this point however, and because the void fraction is relatively high it is difficult to monitor the individual temperature of each phase hence the measured value corresponds in effect to the mixture temperature at each abscissa. This should explain the later deviations between the theoretical and experimental profiles as illustrated in Fig. 16.

Again, no experimental points were included for the dispersed phase temperatures in account of the difficulty to measure firstly the droplet temperatures and later those of the bubbles. Nevertheless, it can be noted that the measured outlet temperature of each phase corresponds to the theoretical value.

Due to this attendant difficulty, the validation of this model goes by a parametric study similar to the one presented above.

Figure 17 compares the theoretical and experimental variations of the continuous phase outlet temperatures vs the continuous phase flow rates where a good agreement can be observed. Moreover, this model predicts satisfactorily the mean void fraction as shown in Fig. 16.

When the void fraction $\alpha(z)$ exceeds 0.3 however, the theoretical values deviate from the experimental values. This disagreement can be explained by coalescence between the bubble–droplet in the exchange column. The present phenomenon was not taken into account by the model.

CONCLUSION

The theoretical analysis with the aid of the experiments of ref. [14] concerning the vaporization of a bubble–droplet showed that the effective heat exchange area is an important parameter in this phenomenon. Experimental and calculated velocity profiles are in good agreement when the effective exchange area is determined.

An analysis of compound multiphase droplets allowed us the prediction of its most probable configuration. This configuration plays an important rôle in the heat exchange processes.

By a mechanistic approach when the bubble–droplet remains attached we showed that this effective area results from the mechanical equilibrium of the bubble–droplet. This equilibrium is supposed to be defined by surface forces. Consideration of the buoyancy effects in addition to the interfacial tension forces must lead to a more precise estimation of the liquid–liquid area.

The study of the dragging phenomenon shows that the continuous phase is carried out in vapour form. The maximum value of the dragging coefficient was estimated and compared to the experimental value. A good agreement was observed at high values of the dispersed phase flow rate or continuous phase temperature in accordance with the assumptions. The experimental setup led us to derive the influence of the several parameters on the behaviour of this type of evaporator. The volumetric heat exchange coefficient obtained differs with the couple of fluids. For refrigerant R113–water it is a maximum of 45 kW m^{-3} °C^{-1}

and about 120 kW m^{-3} $°C^{-1}$ for the n-pentane–water system. The absence of recirculation zones in the column explains the better performance of the latter couple.

An approach in terms of characteristic transfer times lead to a correlation between the thermal performance (efficiency, volumetric heat transfer coefficient) and the evaporator parameters.

The design and sizing of this type of evaporator requires a realistic model. We have presented a model which describes correctly the hydrodynamic and thermal transfers of a vaporizing drop. We have used this model to describe a multidroplet flowing system. The results obtained were satisfactorily compared with our experiments on a spray column using an n-pentane–water couple when the void fraction does not exceed 0.3. At higher values this analysis demonstrates the necessity of taking into account the phenomenon of coalescence between the bubble–droplets.

REFERENCES

1. P. Seguin, R, Santini, L. Tadrist, F. Thiebaut et J. Pantaloni, Réalisation d'un échangeur à contact direct sel fondu-huile couplé à un ensemble de stockage par chaleur latente, *Revue Gén. Therm.* **254,** 189–193 (1983).
2. L. Tadrist, P. Seguin, R. Santini, J. Pantaloni and A. Bricard, Experimental and numerical study of direct contact heat exchangers, *Int. J. Heat Mass Transfer* **28,** 1215–1227 (1985).
3. P. F. Ellis, Geothermal materials survey, Arkansas power and light development and demonstration project. 100 kW power system using direct contact heat exchangers, El-Dorado, Arkansas, Report DOE/ET/27026-T4 (1980).
4. A. Hlinak, T. Lee, J. Lobach, K. Nichols and R. Olander, 500 kW DCHX pilot plant evaluation testing, Lawrence Berkeley Laboratory, U.S. Dept. of Energy (1981).
5. L. Tadrist, I. Shehu-Diso, R. Santini et J. Pantaloni, Etude d'un évaporateur à contact direct, *Revue Gén. Therm.* **279,** 305–307 (1985).
6. J. D. Wright, Sizing of direct-contact preheaters/boilers for solar pond power plant, U.S. Dept. of Energy, Contract EG-77-C-01-4042 (1982).
7. J. L. Honegger, Valorisation thermodynamique de la géothermie moyenne température: simulation d'un échangeur à contact direct co-courant, Thèse de 3ème cycle, Université d'Orléans, Orléans, France (1984).
8. C. R. Wilke, C. T. Cheng, V. L. Ledesma and J. W. Porter, Direct contact heat transfer for sea water evaporation, *Chem. Engng Prog.* **59**(12), 69–75 (1963).
9. S. Sideman and Y. Gat, Direct contact heat transfer with change of phase: spray column studies of a three-phase heat exchanger, *A.I.Ch.E. Jl* **12**(2), 296–303 (1966).
10. R. C. Smith, W. M. Rohsenow and M. S. Kazimi, Volumetric heat-transfer coefficients for direct contact evaporation, *J. Heat Transfer* **104,** 264–303 (1982).
11. M. Blander and D. Hengstenberg, Bubble nucleation in n-pentane, n-hexane + hexadecane mixtures and water, *J. Phys. Chem.* **75**(23), 3613–3619 (1971).
12. Y. H. Mori and K. Komotori, Boiling of single superheated drops in an immiscible liquid, *Heat Transfer—Jap. Res.* **5,** 75–95 (1976).
13. V. P. Skripov, *Metastable Liquids.* Wiley, New York (1974).
14. S. Sideman and Y. Taitel, Direct-contact heat transfer with change of phase: evaporation of drops in an immiscible liquid medium, *Int. J. Heat Mass Transfer* **7,** 1273–1289 (1964).
15. Y. Tochitani, Y. H. Mori and K. Komotori, Vaporization of single liquid drops in an immiscible liquid, Part I: forms and motions of vaporizing drops, *Wärme- und Stoffübertragung* **10,** 51–59 (1977).
16. L. Gradon and A. Selecki, Evaporation of a liquid drop immersed in another immiscible liquid. The case of $\sigma_c < \sigma_d$, *Int. J. Heat Mass Transfer* **20,** 459–466 (1977).
17. K. L. Pinder, Surface area prediction for two phase drops in an immiscible liquid, *Can. J. Chem. Engng* **58,** 318–324 (1980).
18. P. Battya, V. R. Raghavan and K. N. Seetharamu, Parametric studies on direct contact evaporation of a drop in an immiscible liquid, *Int. J. Heat Mass Transfer* **27,** 263–272 (1984).
19. C. B. Prakash and K. L. Pinder, Direct contact heat transfer between two immiscible liquids during vaporization, Part I: measurements of heat transfer coefficient, *Can. J. Chem. Engng* **45,** 210–220 (1967).
20. E. Ruckenstein, On heat transfer between vapour bubbles in motion and the liquid from which they are generated, *Chem. Engng Sci.* **10,** 22–30 (1959).
21. Y. Tochitani, Y. H. Mori and K. Komotori, Vaporization of single liquid drops in an immiscible liquid, Part II: heat transfer characteristics, *Wärme- und Stoffübertragung* **10,** 71–79 (1977).
22. M. R. Mokhtarzadeh and A. A. El-Shirbini, A theoretical analysis of evaporating droplets in an immiscible liquid, *Int. J. Heat Mass Transfer* **22,** 27–38 (1979).
23. A. Selecki and L. Gradon, Equation of motion of an expanding vapour drop in an immiscible liquid medium, *Int. J. Heat Mass Transfer* **19,** 925–929 (1976).
24. G. Ryskin and L. G. Leal, Numerical solution of free-boundary problems in fluid mechanics, Part 2: buoyancy-driven motion of a gas bubble through a quiescent liquid, *J. Fluid Mech.* **148,** 19–35 (1984).
25. F. Odar and W. S. Hamilton, Forces on a sphere accelerating in a viscous fluid, *J. Fluid Mech.* **18,** 302–314 (1964).
26. W. L. Haberman and R. K. Morton, An experimental study of bubbles moving in liquids, *Trans. Am. Soc. Civ. Engrs* **121,** 227–252 (1956).
27. G. K. Raina and P. D. Grover, Direct contact heat transfer with change of phase: theoretical model, *A.I.Ch.E. Jl* **28,** 515–517 (1982).
28. F. Castex, Instabilites de jet dans un système liquide–liquide. Analyse spectrale de l'état vibratoire et corrélation avec la taille des gouttes, Thèse de 3ème cycle, Université de Provence, Marseille, France (1984).
29. G. Hetsroni, *Handbook of Multiphase Systems.* McGraw-Hill, New York (1982).
30. R. Clift, J. R. Grace and M. E. Weker, *Bubbles, Drops and Particles.* Academic Press, New York (1978).

VAPORISATION D'UN LIQUIDE PAR CONTACT DIRECT DANS UN AUTRE LIQUIDE NON MISCIBLE. PARTIE I: VAPORISATION D'UNE GOUTTE. PARTIE II: VAPORISATION D'UN ENSEMBLE DE GOUTTES EN MOUVEMENT

Résumé—Le présent texte porte sur l'étude des évaporateurs à contact direct dans lequel une phase liquide dispersée sous forme de gouttes vaporise au contact d'un autre liquide non miscible plus chaud. Une étude de la vaporisation d'une goutte et d'un ensemble de gouttes en écoulement dans un autre liquide est réalisée. Un formalisme est développé pour déterminer la surface effective d'échange d'une goutte-bulle qui vaporise en écoulement. Les résultats obtenus sont en bon accord avec les expériences. L'étude de l'équilibre mécanique d'une goutte et de sa bulle est réalisée en ne prenant en compte que les forces de tensions interfaciales. Les résultats obtenus sont comparés à l'expérience. Dans une seconde partie une étude expérimentale d'un évaporateur à contact direct est réalisée. Les résultats obtenus ont permis de dégager l'influence des divers paramètres sur son fonctionnement et ses performances. Une étude en termes de temps caractéristiques est developpée en vue de permettre le dimensionnement de ce type d'évaporateurs. Enfin une modélisation des transferts dans la colonne d'évaporation pour décrire l'évolution des températures et du taux de vide est proposée. Les résultats théoriques sont comparés à l'expérience.

VERDAMPFUNG EINER FLÜSSIGKEIT DURCH DIREKTEN KONTAKT MIT EINER ANDEREN NICHT MISCHBAREN FLÜSSIGKEIT. TEIL I: VERDAMPFUNG EINES EINZELNEN TROPFENS. TEIL II: VERDAMPFUNG EINES AUFSTEIGENDEN TROPFENSCHWARMS

Zusammenfassung—Die vorliegende Arbeit ist eine experimentelle und theoretische Studie zur Verdampfung von R113 und n-Pentan, welche in eine entgegenströmende Wassersäule dispergiert werden. Die Verdampfung eines einzelnen Tropfens im ruhenden flüssigen Medium und die Verdampfung eines bewegten Tropfenschwarms wurden untersucht. Eine Methode zur Bestimmung der effektiven Austauschfläche eines aufsteigenden Blasen–Tropfens in der nicht mischbaren Flüssigkeit wurde entwickelt. Die berechneten Ergebnisse stimmen gut mit dem Experiment überein. Das mechanische Gleichgewicht eines Blasen–Tropfens wurde unter ausschließlicher Betrachtung der Oberflächenspannung untersucht. Experimentelle Parameterstudien zum Verhalten des Direkt-Kontakt-Verdampfers werden vorgestellt. Eine Dimensionsanalyse, basierend auf der charakteristischen Übertragungszeit, wurde durchgeführt. Daraus wurden Korrelationen zur Bestimmung des volumetrischen Wärmedurchgangskoeffizienten und des Austausch-Wirkungsgrades entwickelt. Für einen strömenden Tropfenschwarm wird ein analytisches Modell vorgeschlagen, womit der sich entwickelnde Dampfanteil und die Temperatur der an der Austauschsäule vorbeiströmenden Fluide berechnet werden kann. Die Experimente werden mit den numerischen Ergebnissen verglichen.

ИСПАРЕНИЕ ЖИДКОСТИ, НАХОДЯЩЕЙСЯ В НЕПОСРЕДСТВЕННОМ КОНТАКТЕ С ДРУГОЙ НЕСМЕШИВАЮЩЕЙСЯ ЖИДКОСТЬЮ. ЧАСТЬ I: ИСПАРЕНИЕ ОТДЕЛЬНОЙ КАПЛИ. ЧАСТЬ II: ИСПАРЕНИЕ ВСПЛЫВАЮЩИХ КАПЕЛЬ

Аннотация—Представлено экспериментальное и теоретическое исследование процесса испарения при прямом контакте хладагента R113 и n-пентана, диспергированных в колонне при течении воды в противотоке. Изучалось испарение отдельной капли в неподвижной жидкой среде, а также испарение потока капельной жидкости. Получены формулы для определения эффективной поверхности массообмена капли–пузырька, всплывающего в несмешивающейся жидкости. Найдено, что численные результаты хорошо согласуются с экспериментальными данными. Проведено исследование механического равновесия в системе капля–пузырек с учетом только сил поверхностного натяжения. Дано объяснение результатов предыдущего анализа оценок площади поверхности жидкость–жидкость. Экспериментально исследовано влияние различных параметров на характер испарения при прямом контакте. Проведен анализ характерных времен переноса с помощью метода размерностей. Получены критериальные соотношения для определения объемного коэффициента теплообмена, а также интенсивность переносов. Предложена аналитическая модель для капельной жидкости, которая позволяет проследить зволюцию паросодержания и температуры каждой жидкости по высоте колонны. Проведено сравнение экспериментальных и расчетных данных.